frontiers in Microbiology

ORIGINAL RESEARCH
published: 16 November 2021
doi: 10.3389/fmicb.2021.790742

Structure, Function and Regulation of a Second Pyruvate Kinase Isozyme in *Pseudomonas aeruginosa*

*Yassmin Abdelhamid[1], Meng Wang[1], Susannah L. Parkhill[1], Paul Brear[1], Xavier Chee[2], Taufiq Rahman[2] and Martin Welch[1]**

[1] Department of Biochemistry, University of Cambridge, Cambridge, United Kingdom, [2] Department of Pharmacology, University of Cambridge, Cambridge, United Kingdom

Pseudomonas aeruginosa (PA) depends on the Entner-Doudoroff pathway (EDP) for glycolysis. The main enzymatic regulator in the lower half of the EDP is pyruvate kinase. PA contains genes that encode two isoforms of pyruvate kinase, denoted $PykA_{PA}$ and $PykF_{PA}$. In other well-characterized organisms containing two pyruvate kinase isoforms (such as *Escherichia coli*) each isozyme is differentially regulated. The structure, function and regulation of $PykA_{PA}$ has been previously characterized in detail, so in this work, we set out to assess the biochemical and structural properties of the $PykF_{PA}$ isozyme. We show that $pykF_{PA}$ expression is induced in the presence of the diureide, allantoin. In spite of their relatively low amino acid sequence identity, $PykA_{PA}$ and $PykF_{PA}$ display broadly comparable kinetic parameters, and are allosterically regulated by a very similar set of metabolites. However, the x-ray crystal structure of $PykF_{PA}$ revealed significant differences compared with $PykA_{PA}$. Notably, although the main allosteric regulator binding-site of $PykF_{PA}$ was empty, the "ring loop" covering the site adopted a partially closed conformation. Site-directed mutation of the proline residues flanking the ring loop yielded apparent "locked on" and "locked off" allosteric activation phenotypes, depending on the residue mutated. Analysis of $PykF_{PA}$ inter-protomer interactions supports a model in which the conformational transition(s) accompanying allosteric activation involve re-orientation of the A and B domains of the enzyme and subsequent closure of the active site.

Keywords: bacterial metabolism, Entner-Doudoroff pathway, glycolysis, *Pseudomonas aeruginosa*, pyruvate kinase, pykF, x-ray crystallography

OPEN ACCESS

Edited by:
Haike Antelmann, Freie Universität Berlin, Germany

Reviewed by:
Aneta Agnieszka Bartosik, Polish Academy of Sciences, Poland
Karel Olavarria Gamez, Delft University of Technology, Netherlands
Agnieszka J. Pietrzyk-Brzezinska, Lodz University of Technology, Poland

****Correspondence:***
Martin Welch
mw240@cam.ac.uk

Specialty section:
This article was submitted to Microbial Physiology and Metabolism, a section of the journal Frontiers in Microbiology

Received: *07 October 2021*
Accepted: *26 October 2021*
Published: *16 November 2021*

Citation:
Abdelhamid Y, Wang M, Parkhill SL, Brear P, Chee X, Rahman T and Welch M (2021) Structure, Function and Regulation of a Second Pyruvate Kinase Isozyme in Pseudomonas aeruginosa. Front. Microbiol. 12:790742. doi: 10.3389/fmicb.2021.790742

INTRODUCTION

Pseudomonas aeruginosa (PA) is a well-known opportunistic human pathogen and is associated with airway, burn wound, opthalmic and other soft-tissue infections (Preston et al., 1997; Martínez-Solano et al., 2008; Turner et al., 2014). Although it can readily consume glucose, PA does not encode the Embden-Meyerhof-Parnas (EMP) pathway enzyme, phosphofructokinase, and is therefore entirely reliant upon the Entner-Doudoroff pathway (EDP) for glycolysis (Kersters and De Ley, 1968; Lessie and Phibbs, 1984; Temple et al., 1998). The enzymatic logic of the EMP and the EDP are broadly similar; glucose is taken up and phosphorylated, and, following a series of downstream transformations distinct to each pathway, the product is cleaved in a reverse

aldol condensation reaction to yield two three-carbon compounds. However, the substrate of the aldol cleavage is different; in the case of the EMP, fructose 1,6-*bis*phosphate is cleaved to yield glyceraldehyde 3-phosphate (G3P) and dihydroxyacetone phosphate, whereas in the EDP, 2-*keto*-3-deoxy-6-phosphogluconate (KDPG) is cleaved to yield G3P and pyruvate (Kovachevich and Wood, 1955a,b; Drechsler et al., 1959; Peekhaus and Conway, 1998). In both the EMP and the EDP, the metabolic fate of G3P following the aldol cleavage step is identical. The pathways can therefore be conveniently divided into distinct "upper reactions" (which precede the aldol cleavage) and a common set of "lower reactions."

Pyruvate kinase [ATP:pyruvate 2-*O*-phosphotransferase (EC 2.7.1.40)] catalyzes the interconversion of phospho*enol*pyruvate and pyruvate in the final reaction of the "lower half" of EDP and EMP glycolysis, and is widely regarded as the main regulatory enzyme for this sequence of reactions (Rose, 1970; Kayne, 1973; Seeholzer et al., 1991; Al-Zaid Siddiquee et al., 2004; Bücker et al., 2014; Noy et al., 2016).

$$\text{phospho}\textit{enol}\text{pyruvate} + \text{ADP} \leftrightarrow \text{pyruvate} + \text{ATP}$$

Pseudomonas aeruginosa is among a subset of bacteria that express two distinct pyruvate kinase isoforms, denoted PykA and PykF (Waygood et al., 1975, 1976; Garcia-Olalla and Garrido-Pertierra, 1987; Hofmann et al., 2013; Abdelhamid et al., 2019). Both isozymes catalyze the same reaction. We previously demonstrated that PykA displays potent K-type allosteric activation by glucose 6-phosphate (G6P), fructose 6-phosphate (F6P), G3P and by intermediates of the reductive pentose phosphate pathway (PPP) (Abdelhamid et al., 2019). It is important to note here that in PA, the upper half of the EDP and the upper half of the gluconeogenic pathway (encoding the aldolase, fructose 1,6-*bis*phosphatase, and phosphoglucoisomerase) do not operate as essentially parallel "contraflow" reactions, but instead, engage in an integrated cyclical series of reactions; the "Entner-Doudoroff-Embden-Meyerhof-Parnas" (EDEMP) cycle (Nikel et al., 2015; Kohlstedt and Wittmann, 2019). The PPP also feeds intermediates into the EDEMP cycle. Given that PPP intermediates strongly activate PykA, this suggests that flux through the lower half of the EDP is coordinated with the level of intermediates in the EDEMP cycle. Interestingly, the G6P-binding site in *P. aeruginosa* PykA (hereafter, $PykA_{PA}$) is clearly distinct from the G6P-binding site in pyruvate kinase from *Mycobacterium tuberculosis*, indicating remarkable plasticity in the mechanism(s) underpinning allosteric regulation in each enzyme (Zhong et al., 2017; Abdelhamid et al., 2019). On the other hand, the structure, activity and regulation of *P. aeruginosa* PykF (hereafter, $PykF_{PA}$) has not yet been characterized.

Like PA, *Escherichia coli* also contains genes that encode PykA and PykF isozymes. In *E. coli*, both isozymes are expressed, although PykF is generally considered to be the dominant isozyme during aerobic growth, whereas PykA appears to play an important role following oxygen limitation (Ponce et al., 1995; Zhao et al., 2017). The *E. coli* enzymes are differentially regulated; fructose 1,6-*bis*phosphate strongly activates PykF, whereas ribose 5-phosphate (R5P) and adenosine 5′-monophosphate (AMP) activate PykA. However, this functional distinction does not easily translate to "sequence space" and there are no obvious sequence motifs that can be used to differentiate these two classes of isozyme. This raises the question of whether $PykF_{PA}$ might be regulated differently compared with $PykA_{PA}$.

$PykF_{PA}$ shares just 37% amino acid identity with $PykA_{PA}$, and 36% identity with *E. coli* PykF. Given the relatively low level of similarity between $PykF_{PA}$ and other well-characterized pyruvate kinases, and the lack of functional insight that can be gleaned from sequence comparisons alone, we set out here to investigate the biochemical and structural properties of this second pyruvate kinase isozyme in PA. Surprisingly, and although $PykF_{PA}$ was regulated by a broadly similar set of compounds as $PykA_{PA}$, its structure–especially around the likely allosteric site for G6P–was different. Structure-guided site-directed mutagenesis of some of the key residues around the sugar ring loop which "guards" the G6P-binding site revealed unexpected subtlety in the allosteric mechanism of the enzyme. Finally, we show that the inter-protomer interfaces in $PykF_{PA}$ are very different from those in PK enzymes from other structurally characterized species, indicative of a potentially novel mechanism underpinning cooperative transitions.

RESULTS

Expression of $PykF_{PA}$

PykF (PA1498) is the terminal ORF in an uncharacterized cluster of five ORFs (PA1498-PA1502, **Figure 1A**). We previously demonstrated that there is no appreciable PykF expression during growth on glucose, acetate or glycerol as sole carbon sources (Abdelhamid et al., 2019). However, the presence of a probable glyoxylate carboligase (PA1502) and a putative tartronate semialdehyde reductase (PA1500) in the same gene cluster as *pykF* led us to suspect that the cluster may be involved in the terminal steps of allantoin (glyoxyldiureide, **Figures 1B,C**) catabolism (Cusa et al., 1999). We therefore wondered whether PykF expression might be induced in the presence of allantoin. To test this, we grew cultures (separately) of wild-type PA (strain PAO1), an isogenic *pykA* mutant, and an isogenic *pykF* mutant, in M9 minimal medium containing either glucose, allantoin, or glucose plus allantoin as a sole carbon source. Aliquots of the cultures were analyzed by Western blotting using antibodies raised against purified PykA or purified PykF, as previously described (Abdelhamid et al., 2019). PykA was expressed during growth on all of the tested carbon sources in the wild-type and in the *pykF* mutant, but was not detectable in the *pykA* mutant, as expected (**Figure 1D**). PykF was undetectable in cells grown on glucose as a sole carbon source [as previously reported (Abdelhamid et al., 2019)] but was expressed in cells grown on media containing allantoin (**Figure 1D**). This expression of PykF in the presence of allantoin was abolished in the *pykF* mutant, as expected (**Figure 1E**). We conclude that *pykF* expression appears to be induced in the presence of allantoin (although we note that this does not exclude the possibility that this

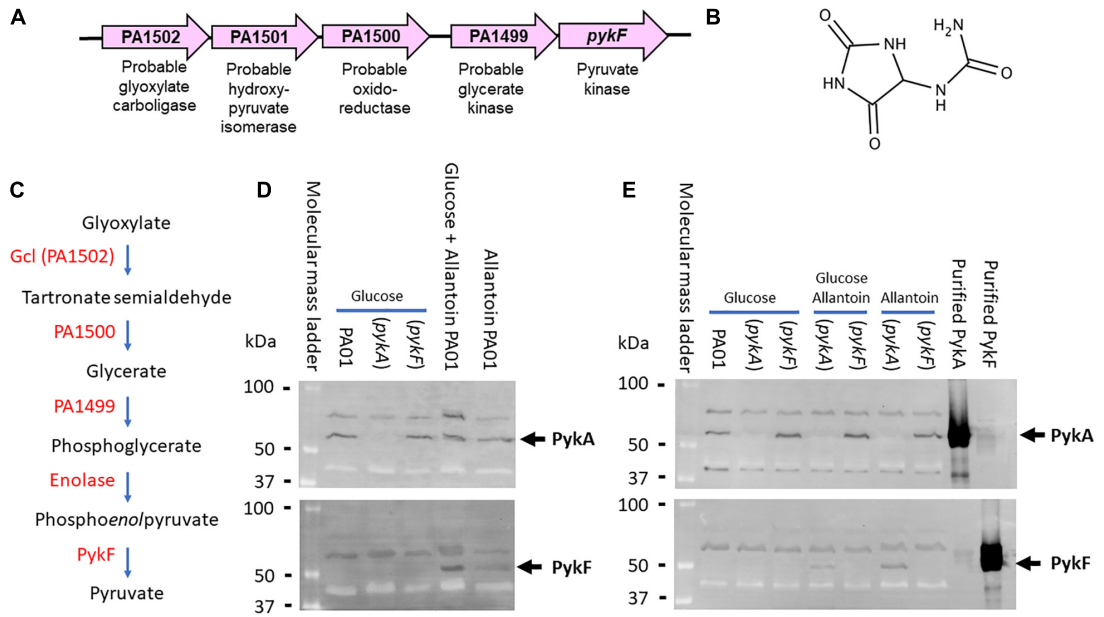

FIGURE 1 | Genetic context and expression of PykF. **(A)** ORFs associated with the PA1489-PA1502 cluster and their predicted function. **(B)** Structure of allantoin. **(C)** Predicted metabolic reactions catalyzed by each encoded enzyme in the gene cluster. Note that glyoxylate and urea are the breakdown products of allantoin degradation. **(D)** PykF is not expressed in wild-type *P. aeruginosa* in the presence of glucose but is expressed in the presence of allantoin. The figure shows western blots of cell extracts of the indicated *P. aeruginosa* derivatives (wild-type PAO1, *pykA* mutant, or *pykF* mutant, as indicated) obtained after overnight growth in M9 medium containing glucose, glucose plus allantoin, or allantoin alone. The blot in the upper panel was probed with anti-PykA antibodies and the blot in the lower panel was probed with anti-PykF antibodies. The identity of the cross-reacting bands with higher molecular mass than PykA or PykF in each panel is not known, but their presence in the *pykA* and *pykF* mutant extracts indicates that they are unrelated to these pyruvate kinases. **(E)** Allantoin-induced PykF expression is abolished in a *pykF* mutant. The figure shows a western blot of cell extracts from a *pykA* or a *pykF* mutant (as indicated) grown in the presence or absence of glucose and/or allantoin (as indicated). To confirm minimal cross-reactivity of the antibodies, purified PykA or PykF (as indicated) were loaded on the right-hand side of each blot.

cluster of genes may also play a role(s) in other aspects of *P. aeruginosa* physiology too). Interestingly, the *pykF* mutant displayed a marked growth defect when grown on allantoin as a sole carbon source (**Supplementary Figure 1**) whereas growth of the *pykA* mutant was unaffected. This suggests that PykA (which is abundantly expressed during growth on allantoin; **Figures 1D,E**) cannot fully substitute for PykF under these circumstances, although we cannot rule out the possibility that the Tn insertion in this terminal ORF may have polar effects on the 3′ end of the cluster too. Current efforts are aimed at confirming the function of each of the other enzymes in the PA1498-PA1502 cluster, and in identifying how allantoin might regulate this cluster at a genetic level. However, the conditional expression of PykF raises the question of why this additional pyruvate kinase isoform is needed at all, especially given the apparently constitutive expression of PykA. One possibility is that $PykF_{PA}$ displays different kinetic or regulatory properties compared with $PykA_{PA}$, so this is what we investigated next.

Kinetic Properties of $PykF_{PA}$

$PykF_{PA}$ was purified as previously described (Abdelhamid et al., 2019). Analytical ultracentrifugation (AUC) analysis revealed that the purified $PykF_{PA}$ [monomeric molecular mass 51.5 kDa (**Figure 2A**)] is a tetramer in solution with a molecular mass of approximately 200 kDa (**Supplementary Figure 2**). Kinetic analyses revealed that $PykF_{PA}$ exhibited a similar kinetic profile toward phospho*enol*pyruvate (PEP) and ADP as most other well-characterized PK enzymes (**Figure 2**). $PykF_{PA}$ displayed sigmoidal kinetics in response to PEP titration, with an $S_{0.5}$ value of 1.03 mM and a Hill coefficient (h) of 2.82, indicative of positive homotropic cooperativity (**Figure 2** and **Table 1**). By contrast, $PykF_{PA}$ displayed Michaelis-Menten (hyperbolic) kinetics in response to ADP titration, with a K_M of 0.11 mM ± 0.01 (**Figure 2**). These $S_{0.5(PEP)}$ and $K_{M(ADP)}$ values for $PykF_{PA}$ were somewhat higher than the previously reported values for $PykA_{PA}$ [$S_{0.5(PEP)}$ = 0.67 mM and $K_{M(ADP)}$ = 0.07 mM (Abdelhamid et al., 2019)], suggesting that $PykF_{PA}$ is intrinsically only slightly less active than $PykA_{PA}$ [For further comparison, the $k_{cat(PEP)}$ and $k_{cat(PEP)}/S_{0.5(PEP)}$ values for $PykF_{PA}$ were 379 s^{-1} and 367 s^{-1} mM^{-1}, whereas the corresponding values for $PykA_{PA}$ were 432 s^{-1} and 644 s^{-1} mM^{-1}, respectively].

All PKs require Mg^{2+} for catalysis, and many also require K^+ in order to achieve maximal activity (Kachmar and Boyer, 1953; Baek and Nowak, 1982). Consistent with this, purified $PykF_{PA}$ was strongly dependent on the presence of Mg^{2+} in the assay mixtures for activity (**Supplementary Figure 3A**). However, monovalent cations (K^+, NH_4^+, and Na^+) did not synergize this activity, and indeed, when present at 100 mM concentration, even had a detrimental effect on the activity of $PykF_{PA}$ (**Supplementary Figures 3B,C**). A similar K^+-independent activity profile was previously observed with purified $PykA_{PA}$ (Abdelhamid et al., 2019) and can be attributed

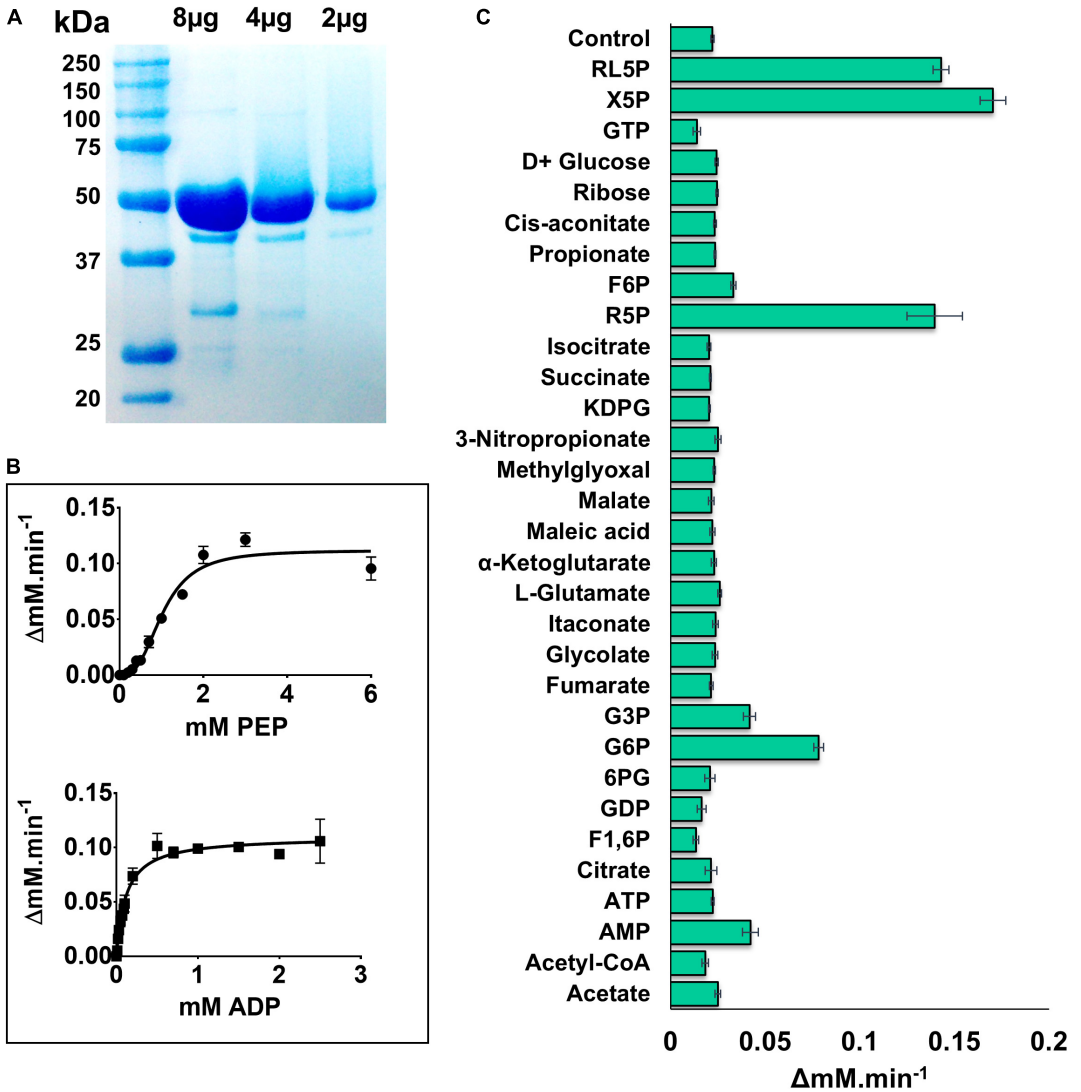

FIGURE 2 | Kinetic characterization of PykF. **(A)** SDS-PAGE gel showing purified, untagged PykF (51.5 kDa). The gel was prepared with 12% (w/v) acrylamide and stained with Coomassie Brilliant Blue G250 [The minor bands at around 30 and 40 kDa molecular mass correspond to degradation products of PykF]. **(B)** PykF kinetics with respect to PEP and ADP. The PEP titration was performed using 2 mM ADP (i.e., a saturating concentration) whereas the ADP titration was performed using 5 mM PEP (also a saturating concentration). The R^2 values for the curve fit to the PEP and ADP titrations were 0.96 in both cases. The 95% confidence interval estimates for the kinetic parameters are shown in **Supplementary Table 4**. **(C)** The effect of different metabolic regulators on PykF activity at low [PEP] (0.3 mM) and 2 mM ADP. Putative regulators were added at 1 mM final concentration, except for R5P, X5P, and RL5P which were used at 0.15, 0.5, and 0.5, respectively. The aim of this experiment was to identify potential activators. Data in panels **(B,C)** represent the mean and standard deviation of three independent experiments.

to the presence of a lysine residue at position 74 in the sequence $G_{72}PKLR_{76}$ ($PykF_{PA}$ numbering, **Supplementary Figure 4**). K^+-dependent PK enzymes generally contain a glutamate residue at the equivalent position (Laughlin and Reed, 1997; Oria-Hernández et al., 2006). $PykF_{PA}$ activity was also supported by Co^{2+} and, to a lesser extent, also by Mn^{2+} (*data not shown*).

Regulation of $PykF_{PA}$

Enteric species such as *E. coli* and *Salmonella enterica* serovar Typhimurium depend primarily on the EMP for glycolysis (Romano and Conway, 1996; Bumann and Schothorst, 2017), and also contain genes encoding two PK isoforms (Valentini et al., 1979; Garcia-Olalla and Garrido-Pertierra, 1987). The PykF isoforms from these species have been found to be strongly activated by fructose 1,6-*bis*phosphate (F1,6BP), the product of phosphofructokinase (Pfk) action (Waygood and Sanwal, 1974; Waygood et al., 1976; Garcia-Olalla and Garrido-Pertierra, 1987). However, PA exclusively uses the EDP for glycolysis, and does not encode *pfk* (although F1,6BP can be generated in this organism through gluconeogenesis). Therefore, it is plausible that $PykF_{PA}$ is regulated differently compared with the enteric isozymes. The activity of $PykF_{PA}$ was measured in the presence of metabolites from the EDP, EMP/gluconeogenesis pathway, TCA cycle, and PPP to identify potential regulatory

TABLE 1 | The effect of metabolic intermediates on PykF activity.

PEP titration	No additive	1 mM G6P	0.15 mM R5P	1 mM AMP	1 mM G3P	0.5 mM X5P	0.5 mM RL5P	Pro455→Ala No G6P	Pro455→Ala + G6P	Pro459→Ala No G6P	Pro459→Ala + G6P	Pro455, Pro459→Ala No G6P	Pro455, Pro459→Ala + G6P
$S_{0.5}$ (mM)	1.03 ± 0.01	0.34 ± 0.04	0.23 ± 0.03	0.56 ± 0.02	0.68 ± 0.02	0.11 ± 0.01	0.17 ± 0.01	0.48 ± 0.02	0.47 ± 0.03	1.11 ± 0.05	0.92 ± 0.07	2.05 ± 0.53	1.90 ± 0.51
Hill Coefficient (h)	2.82 ± 0.27	1.25 ± 0.18	1.47 ± 0.32	2.03 ± 0.15	2.69 ± 0.17	1.58 ± 0.21	2.15 ± 0.24	1.65 ± 0.11	1.38 ± 0.13	3.91 ± 0.66	2.63 ± 0.44	1.07 ± 0.18	1.09 ± 0.14
V_{max} (ΔmM.min^{-1})	0.11 ± 0.00	0.13 ± 0.01	0.14 ± 0.01	0.11 ± 0.00	0.09 ± 0.00	0.13 ± 0.00	0.13 ± 0.00	0.06 ± 0.00	0.06 ± 0.00	0.04 ± 0.00	0.04 ± 0.00	0.04 ± 0.00	0.04 ± 0.00
k_{cat} (s^{-1})	378.6	446.7	515.4	365.6	316.2	432.9	439.8	249.6	249.6	126.9	151.6	146.7	154.7
$k_{cat}/S_{0.5}$ (s^{-1}.mM^{-1})	367	1314	2241	653	465	3935	2587	522	530	114	165	72	81

Kinetic parameters were calculated using GraphPad Prism from best-fit non-linear regression analysis of the data. Abbreviations: R5P, ribose 5-phosphate; G6P, glucose 6-phosphate; AMP, adenosine 5′ monophosphate; G3P, glyceraldehyde 3-phosphate; X5P, xylulose 5-phosphate; RL5P, ribulose 5-phosphate. k_{cat} was calculated using [E_t] = [PykF monomer]. All regulators were added at 1 mM final concentration except R5P, X5P and RL5P which were used at 0.15, 0.5, and 0.5 mM, respectively.

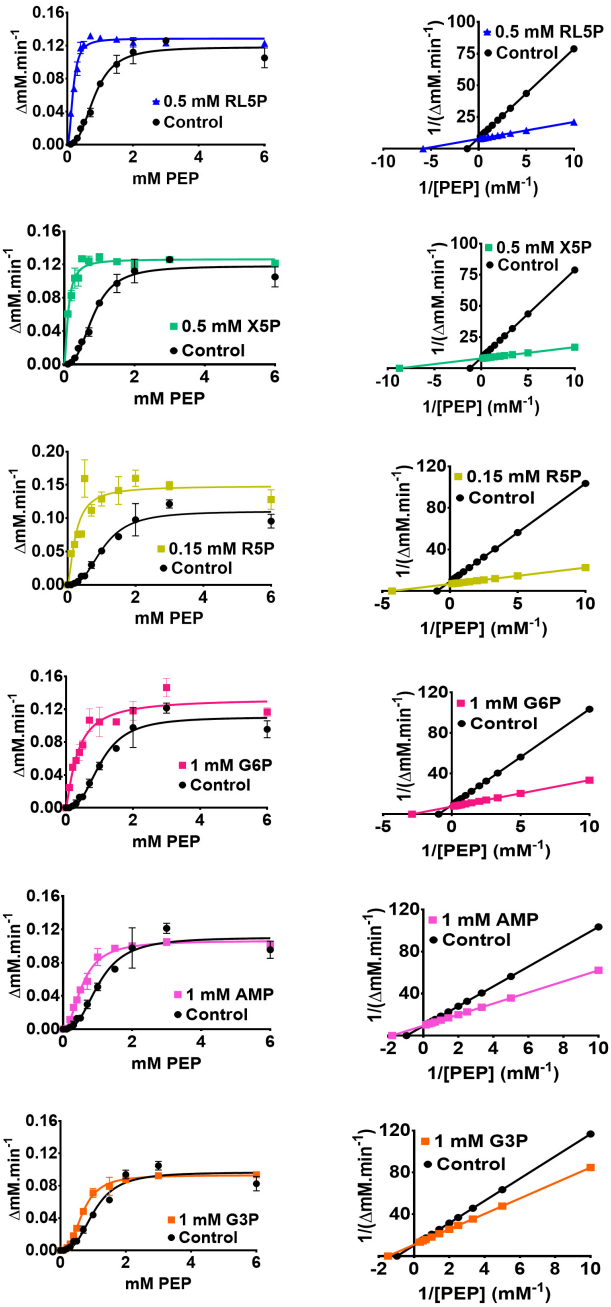

FIGURE 3 | The metabolic regulation of PykF. (Left panel) Michaelis-Menten plots showing that the indicated regulators primarily convert PykF from sigmoidal to hyperbolic kinetics. Data represent the mean and standard deviation of three independent experiments. (Right panel) Lineweaver-Burk plots showing that the indicated regulators primarily act to decrease $S_{0.5}$ of PykF compared with the control. "Control" indicates the reaction kinetics in the absence of added regulators. The changes in PykF kinetic constants elicited by each regulator are shown in **Table 1**. The 95% confidence interval estimates for the kinetic parameters are provided in **Supplementary Table 4**.

molecules. $PykF_{PA}$ was not activated by F1,6BP (**Figure 2C**), but was strongly activated by metabolites from the non-oxidative PPP [(xylulose 5-phosphate (X5P), ribulose 5-phosphate (RL5P),

and R5P], and also, to a lesser extent, by the EDP intermediates G6P and G3P (**Figure 2C**). The same set of regulators also activate $PykA_{PA}$ (Abdelhamid et al., 2019). However, there were some differences between the enzymes. For example, $PykF_{PA}$ (but not $PykA_{PA}$) was activated by AMP whereas F6P and KDPG, which are activators of $PykA_{PA}$, had little effect on $PykF_{PA}$.

Detailed analysis of these regulators (which all appeared to be "K-type activators," affecting $S_{0.5}$ rather than k_{cat}) revealed that the PPP metabolites were the most potent activators (**Table 1** and **Figure 3**). In the presence of these compounds, the sigmoidal PEP kinetics of $PykF_{PA}$ became more Michaelis-Menten-like (hyperbolic), as indicated by the decreased Hill coefficient (h) compared with the control. The ADP-dependency of $PykF_{PA}$ was unaffected by these compounds (**Supplementary Figure 5**).

TABLE 2 | Crystallographic data collection and refinement statistics of PykF.

PDB code	7OO1
Synchrotron/X-ray source	Diamond Light Source
Beamline	IO4-1
Data collection	
Wavelength (Å)	0.9159
Resolution range (Å)	115.14–3.01 (3.09–3.01)
Space group	*P*3 2 1
Unit cell	
a, *b*, *c*, (Å)	169.05, 169.05, 115.11
α, β, γ (°)	90, 90, 120
Total reflections	1772874
Unique reflections	37859
Multiplicity	46.8 (21.2)
Completeness (%)	99.7 (94.0)
Mean *I*/sigma (*I*)	16.3 (1.2)
Wilson B-factor	115.96
R-merge	0.139 (3.01)
R-meas	0.140 (3.09)
CC1/2	1.000 (0.85)
Refinement	
Resolution range (High res) (Å)	73.20–3.01 (3.09–3.01)
Reflections used in refinement	37564 (2728)
Reflections used for R-free	1859 (108)
R-work	0.24 (0.51)
R-free	0.29 (0.47)
Number of molecules in the ASU:	2
Number of non-hydrogen atoms	
Macromolecules	7213
Ligands	N/A
Protein residues	
RMS (bonds) (Å)	0.01
RMS (angles) (°)	1.6
Ramachandran favored (%)	94
Ramachandran allowed (%)	6.0
Ramachandran outliers (%)	0.1
Average B-factor	
Macromolecules	124
Ligands	N/A
Solvent	N/A

Values in parentheses are for the highest resolution shell. N/A: Not applicable.

Structural Features of $PykF_{PA}$

To further investigate the possible differences between $PykA_{PA}$ and $PykF_{PA}$, we determined the x-ray crystal structure of untagged full-length (477 residues) $PykF_{PA}$ to 3.01 Å resolution (PDB 7OO1). Attempts to improve this resolution through fine screening around the best crystallization conditions, or through the use of crystallization additives, were unsuccessful. However, at 3.01 Å resolution, most of the important structural features could be assigned. The crystallization and diffraction statistics are provided in **Table 2**. **Table 3** summarizes the main structural differences between $PykF_{PA}$ and other published bacterial PK structures. Interestingly, $PykF_{PA}$ has least amino acid sequence identity with pyruvate kinase isoform F from *E. coli* ($PykF_{EC}$) and is structurally different to $PykA_{PA}$. The asymmetric unit of $PykF_{PA}$ consisted of two protomers (chain A and chain B) and a complete tetramer was generated by symmetry with chains C and D (**Figure 4**). Each protomer comprised three domains (denoted A, B, and C) and the tetramer contained four inter-protomer interfaces; two A-A interfaces (between adjacent A-domains), and two C-C interfaces (between adjacent C-domains) (**Figure 4**). The enzyme was modeled in the apo-form and attempts at obtaining diffracting crystals with bound regulator molecules were unsuccessful.

The A-domain comprises an eight α/β TIM barrel-like structure with the α-helices spanning around a core of β-strands. Similar to $PykA_{PA}$, Aα6 and Aα8 are preceded by shorter helical segments; denoted as Aα6′ and Aα8′, respectively. The Aα6′ helix contains the active site signature motif (M_{238}VARGDLGVE$_{247}$) (**Supplementary Figure 4**). As in other pyruvate kinases, the A domain was flanked on the C-terminal side by the B domain and on the N-terminal side by the C-domain. The B-domain comprises seven β-strands and a small α-helix, whereas the C-domain is formed of four α-helices alternating with five β-strands. Although the arrangement of secondary structures in the C-domain of $PykF_{PA}$ is generally similar to that in $PykA_{PA}$ and $PykF_{EC}$, $PykF_{PA}$ contained an additional structure denoted Cα1′ (**Figure 4**). Cα1′ is a short helix spanning Tyr338–Glu343 and precedes the longer Cα1 helix (**Figure 4** and **Supplementary Figure 4**). Cα1′ is important because it is integrally associated with the A-A interface.

Amino acid sequence analysis shows that the active site of $PykF_{PA}$ is comprised of strictly conserved residues (**Supplementary Figure 4**). Superposition of these active site residues in $PykF_{PA}$ (no bound substrate, PDB 7OO1), $PykA_{PA}$ (bound to a substrate analog, malonate-Mg^{2+}, PDB 6QXL), and $PykF_{EC}$ (no bound substrate, PDB 1PKY) revealed that the constellation of the active site residues in $PykF_{PA}$ (comprised of the side chains from Arg35, Lys217, Glu219, Gly242, Asp243, and Thr275) adopts a similar configuration in the active (holo) structure, represented by PDB:6QXL, and in the inactive (apo) structure, represented by PDB:1PKY (**Supplementary Figure 6**). The only residue in the active site constellation of $PykA_{PA}$ that can be said to adopt a significantly different configuration between the inactive and active structures is

TABLE 3 | A comparison between $PykF_{PA}$ and other bacterial pyruvate kinase structures in the Protein Data Bank.

	Amino acid sequence identity with $PykF_{PA}$	Cα1′ helix (or similar)	Elongated Aα5-Aβ5 loop at the active site	Extra C-terminal sequence
P. aeruginosa PykF (Q9I3L4)	100%	+	–	–
B. stearothermophilus Pyk (Q02499)	42%	+	–	+
M. tuberculosis Pyk (P9WKE5)	40.5%	–	–	–
S. aureus Pyk (Q6GG09)	37.6%	+	–	+
P. aeruginosa PykA (Q9HW72)	37%	–	+	–
E. coli PykF (P0AD61)	36%	–	–	–

The pyruvate kinase isoforms are identified using their gene names and UniProt IDs.

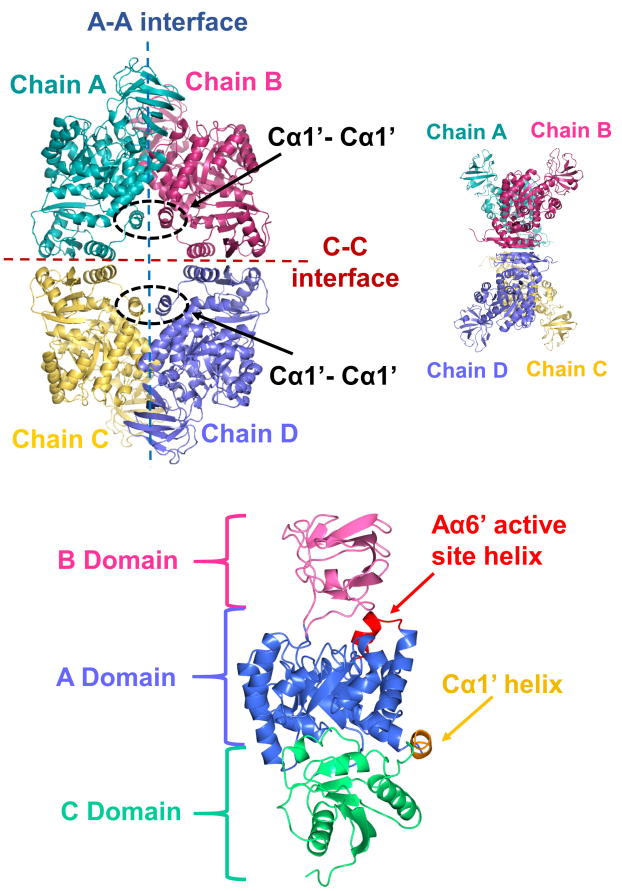

FIGURE 4 | X-ray crystal structure of PykF. (Top diagrams) Front and side views of the PykF homotetramer. Chain A and B were already present in the asymmetric unit of PykF, whereas chains C and D were generated using symmetry coordinates. The A-A and the C-C interfaces are shown. The Cα1′ helices across the A-A interface are shown in dashed ovals. (Bottom diagram) Domain organization of a PykF subunit. A-, B- and C-domains of PykF are colored in blue, pink, and green, respectively. The active site helix and Cα1′ are colored in red and orange, respectively.

Asp243 in $PykF_{PA}$. In the substrate bound (active) structure, 6QXL, this residue re-orients away from the active site slightly in order to make space for the Mg^{2+} that is chelated by the substrate (**Supplementary Figure 6**).

In spite of the relatively small differences in the active site configuration between the active and inactive conformers of pyruvate kinase, activation resulted in a large shift in the position of the B-domain relative to the A-domain (**Figures 5A,B**). In the active (substrate bound) configuration, the B-domain clearly rotates toward the A-domain. This rotation causes a partial closing of the entrance to the active site compared with the inactive (no substrate, pdb:7OO1 and 1PKY) configurations (**Figure 5C**). The inactive configuration of the $PykF_{PA}$ active site was further confirmed by analysis of the orientation of the terminal arginine residue (Arg289) in helix Aα7 (**Supplementary Figure 6**). In inactive structures such as $PykF_{EC}$ PDB 1PKY, Arg292 (equivalent to Arg289 in $PykF_{PA}$) interacts with Asp297 (equivalent to Asp294 in $PykF_{PA}$) from the adjacent protomer, forming an Aα7-Aα7 bond. This interaction is preserved in the $PykF_{PA}$ structure presented here. However, in the structure of active $PykA_{PA}$ (PDB 6QXL) Arg296 (equivalent to Arg289 in $PykF_{PA}$) reorients toward the active site helix (Aα6′), forming an Aα7-Aα6′ interaction.

In the previously solved structure of G6P-bound $PykA_{PA}$, the phosphate and sugar ring moieties of G6P are anchored in the allosteric pocket *via* a "phosphate loop" (Cβ1-Cα2 loop) and a "ring loop" (Cβ4-Cβ5 loop), respectively (Abdelhamid et al., 2019). Indeed, closure of the allosteric site by the ring loop has been proposed to accompany binding of G6P (Zhong et al., 2017; Abdelhamid et al., 2019). Surprisingly, superposition of $PykF_{PA}$ (empty allosteric site), $PykA_{PA}$ (PDB 6QXL, G6P bound to allosteric site), and $PykF_{EC}$ (PDB 1PKY, empty allosteric site) revealed that the ring loop in $PykF_{PA}$ adopts an intermediate conformation between the fully "open" configuration seen in $PykF_{EC}$ and the "closed" configuration in $PykA_{PA}$ (**Figure 5D**). This partially closed configuration of the ring loop in apo-$PykF_{PA}$ likely reflects the nature of the amino acids comprising the ring loop (residues 454–461).

Site-Directed Mutagenesis of the Ring Loop in $PykF_{PA}$

Compared with $PykA_{PA}$ and $PykF_{EC}$, the ring loop in $PykF_{PA}$ is unusual because it is flanked by two proline residues, Pro455 and Pro459 (**Figure 5D** and **Supplementary Figure 4**). Although Pro455 is conserved in several pyruvate kinases (**Supplementary Figure 4**), Pro459 is not conserved. Proline residues can impact on the conformational freedom of adjacent amino acids, so we

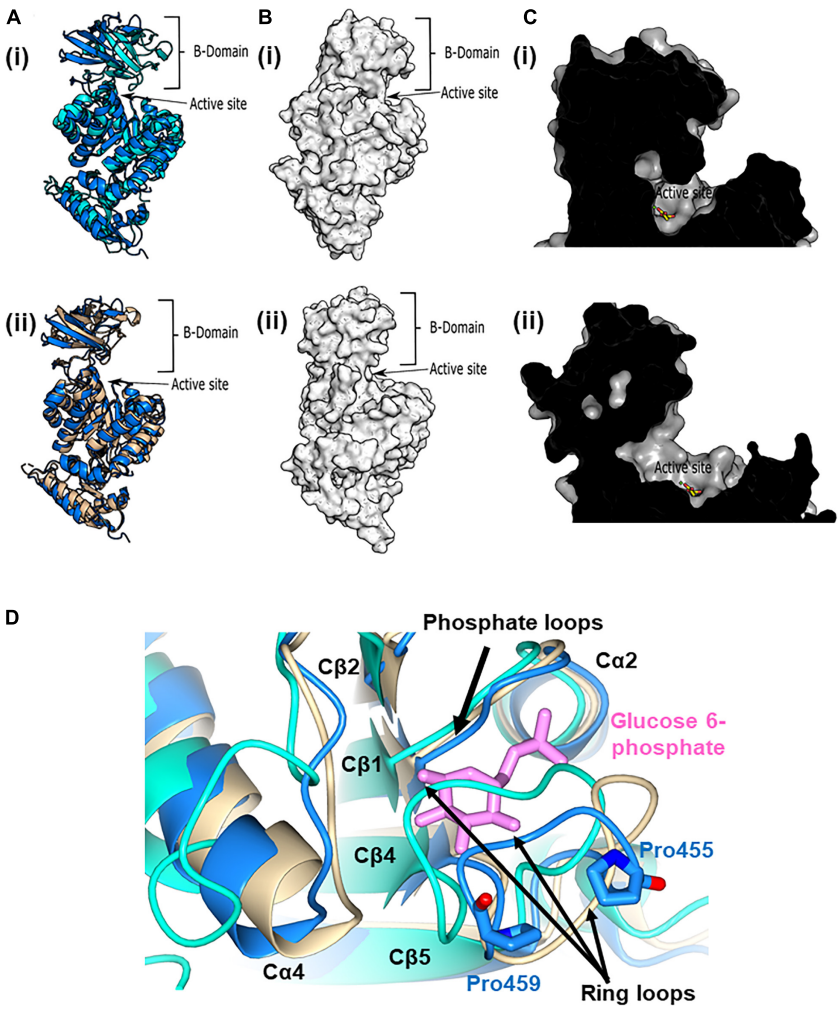

FIGURE 5 | The active and allosteric sites of PykF. **(A)** (i) Cartoon representation of the crystal structure of a presumed inactive conformation of pyruvate kinase ($PykF_{PA}$; 7OO1, blue) overlain onto the crystal structure of a presumed active configuration of the enzyme ($PykA_{PA}$; 6QXL, cyan). (ii) Cartoon representation of the crystal structure of $PykF_{PA}$ (inactive configuration, 7OO1, blue) overlain onto the crystal structure of $PykF_{EC}$ (inactive configuration, 1PKY, yellow). **(B)** Surface representation of the crystal structure of $PykA_{PA}$ [(i) 6QXL] and $PykF_{PA}$ [(ii) 7OO1, blue]. **(C)** (i) Cross-section through the active site of $PykA_{PA}$ (active configuration of the enzyme, 6QXL) The substrate analog, malonate, is shown in yellow. (ii) Cross-section through the active site of $PykF_{PA}$ (inactive configuration of the enzyme, 7OO1). The superimposed binding mode of the malonate from 6QXL is shown in yellow. **(D)** Partial closure of the allosteric site of $PykF_{PA}$. Superposition of the allosteric site in $PykF_{PA}$ (7OO1, blue), $PykF_{EC}$ (1PKY, yellow), and $PykA_{PA}$ (6QXL, cyan) showing disposition of the ring loop of $PykF_{PA}$ toward the allosteric site, probably determined by the configuration of Pro455 and Pro459. The G6P bound to $PykA_{PA}$ is shown as pink sticks.

wondered whether these flanking prolines may alter the flexibility of the loop and perhaps play an important role in dictating the response of the protein to the binding of allosteric regulators [In PykA, structural data indicate that G6P binding pulls the ring loop across the effector binding site, which, in turn, displaces a mobile loop at the end of Cα4. The consequent conformational change is transmitted through the enzyme to the A-A promoter interface, and thence to the active site (Abdelhamid et al., 2019)]. To investigate this further, we used site-directed mutagenesis to mutate Pro455 and Pro459 (separately) to alanine and examined the impact of these changes on the kinetics of the enzyme and its response to G6P. The Pro455Ala mutation increased the activity of the enzyme, with a low $S_{0.5}$ value and Michaelis-Menten (hyperbolic) kinetics irrespective of the presence or absence of G6P, suggesting that enzyme is likely in a more active conformation (**Table 1** and **Supplementary Figure 7A**). By contrast, the Pro459Ala mutation did the opposite, decreasing the activity of the enzyme and favoring a conformation that was only poorly responsive to G6P. The Pro459Ala mutant protein exhibited strongly sigmoidal kinetics in the presence and absence of the regulator (**Table 1** and **Supplementary Figure 7B**). Given the contrasting effects of the Pro→Ala substitutions at each end of the ring loop, we next wondered what would happen if both residues were replaced with Ala in the same protein. The Pro455Ala/Pro459Ala double mutant had a high $S_{0.5(PEP)}$ (1.9–2.0 mM) and displayed essentially no cooperativity (the Hill coefficient, h ≈ 1), irrespective of the presence of G6P (**Table 1** and **Supplementary Figure 7C**). Taken together, these

data indicate that the specific nature of the residues flanking the ring loop has a profound impact on the ability of the enzyme to respond to allosteric regulators.

Inter-Protomer Interactions in $PykF_{PA}$

The A-A interface in $PykF_{PA}$ was formed between the adjacent A-domains from chain A and chain B, and from chain C and D, whereas the C-C interface was present between the adjacent C-domains of chain A and chain C, and of chain B and D (**Figure 4**). Interactions across the A-A and C-C inter-protomer spaces of $PykF_{PA}$ are listed in **Supplementary Table 2**.

The A-A interface of $PykF_{PA}$ comprises Aα6, Aα7, Aα8, Cα1′, the Aα7-Aβ7 loop and the Aα8-Cα1′ loop (**Figure 6**). From analysis of the structure, it appears that the A-A interaction is dominated by the interlocking of Aα6 and Aα7. The Aα7 helix from the first A domain sits in the groove that is formed between Aα6 and Aα7 in the second A domain, with the first residue of Aα7 (Arg289) penetrating deep into the groove and forming a hydrogen bond with Asp294 (**Figure 6D**). Interestingly, the orientation of Arg289 correlates well with the activation state of the protein, and in $PykF_{PA}$, adopts a configuration commensurate with the inactive state (**Supplementary Figure 6B**). The A-A interface is also further stabilized *via* a web of additional potential hydrogen bonds and salt bridges (Lys258-Asp337/Glu335, and Glu251-Lys327) (**Figure 6D** and **Supplementary Table 2**). The Cα1′ helix, which is absent from $PykA_{PA}$ and $PykF_{EC}$, connects the opposing A-domains of $PykF_{PA}$ through a Cα1′-Cα1′ interaction (**Figures 6A,C**). As shown in **Table 3**, the PK isozymes from *Bacillus stearothermophilus* and *Staphylococcus aureus* also contain Cα1′-like helices, similar to $PykF_{PA}$. In $PykF_{PA}$, the Cα1′-Cα1′ interaction is mediated by the side chains of Gln341 from each protomer, which form a glutamine dimer linked by a probable pair of reciprocal hydrogen bonds (3 Å). By contrast, in the *S. aureus* enzyme the Cα1′-Cα1′ interaction is mediated by a salt bridge, whereas in the PK from *B. stearothermophilus* there is no obvious Cα1′-Cα1′ interaction (**Figure 6C**). To test whether the putative Gln341-Gln341 hydrogen bond(s) might play a role in the conformational transitions associated with $PykF_{PA}$ function, we mutated this residue to alanine. However, this had little discernible effect on the kinetics of the enzyme in the presence or absence of G6P (**Supplementary Figure 7D**).

The secondary structures at the C-C interface in $PykF_{PA}$ were similar to those in $PykF_{EC}$ (PDB 1PKY, open allosteric site) (**Figure 7**). The interface is comprised of the α-helices Cα4 and Cα1, which flank Cβ5. The interface is more planar than the A-A interface with no binding pockets or grooves. At the C-C interface of $PykF_{PA}$ and $PykF_{EC}$, Cα4 from one protomer abuts Cα4 of the adjacent protomer, and Cβ5 forms an extended β-sheet with the respective Cβ5 of the adjacent protomer. Additionally, and unlike $PykA_{PA}$, Cα1 and the Cα1-Cα1′ loop (equivalent to loop Aα8-Cα1 in $PykF_{EC}$) from each protomer are not intimately associated in these enzymes, but instead, exhibit only a weak hydrophobic interaction between the helices (**Figure 7**). This configuration at the C-C interface is indicative of an empty allosteric site, as these interactions are re-arranged in G6P-bound $PykA_{PA}$ (**Figure 7**). In $PykA_{PA}$, G6P binding displaces Cα4 concomitantly bringing Cα1 and the Aα8-Cα1 loop closer to the interface (Abdelhamid et al., 2019). Interestingly, and despite its superficial resemblance to the C-C interface in $PykF_{EC}$, the C-C interface of $PykF_{PA}$ contains a number of bonds between non-conserved residues (**Supplementary Figure 4**).

Investigation of inter-protomer interactions can potentially provide insight into the mechanism by which conformational signals are transmitted between the different protomers (Wooll et al., 2001). However, comparison of the inter-protomer interactions between secondary structural elements in the apo structures of $PykF_{PA}$ (PDB 7OO1), $PykF_{EC}$ (PDB 1PKY), and Pyk_{Mtb} (PDB 5WRP) revealed that these interactions are not especially well-conserved between the species (**Figure 8**). The A-A interface in $PykF_{PA}$ is primarily distinguished by bonding of Cα1′ on one protomer with Cα1′ on the other, and by bonding of the Aα8-Cα1′ loop on one protomer with Aα6 on the other (**Figure 8**). These interactions are not present at the A-A interface of $PykF_{EC}$ or Pyk_{Mtb}. On the other hand, both $PykF_{EC}$ and Pyk_{Mtb} exhibit Aα6-Aα7 interactions (absent in $PykF_{PA}$). In $PykF_{EC}$, the Aα6-Aα6′ loop also contributes to the A-A interface–interactions that are again, absent in $PykF_{PA}$. Similarly, the active site helix Aα6′ and parts of the B domain are present at the A-A interface in Pyk_{Mtb}, but not in $PykF_{PA}$. Analysis of the C-C interface reveals a similar story. Compared with $PykF_{EC}$, the C-C interface of $PykF_{PA}$ does not include the ring loop (Cβ4-Cβ5). Absence of the ring loop from the interface in $PykF_{PA}$ is likely related to the conformational constraints introduced by the two proline residues (Pro455 and Pro459) that flank the loop in this enzyme. By contrast, the C-C interface of $PykF_{EC}$ does include the ring loop, but without any salt bridges. In Pyk_{Mtb}, the C-C interface comprises the ring loop, the tail loop, Aα8-Cα1 loop and the Cα1 helix (all absent from the interface in $PykF_{PA}$). The discrepancy between the inter-protomer spaces of $PykF_{PA}$ (on the one hand) and $PykF_{EC}$ or Pyk_{Mtb} (on the other) suggests that $PykF_{PA}$ most likely depends on a distinctive mechanism for allosteric signal transduction compared with previously proposed models.

DISCUSSION

In this work, we characterized the second encoded pyruvate kinase isozyme of PA, $PykF_{PA}$. Based on the presumed function (allantoin catabolism) of the ORFs in the *pykF*-containing cluster, we predicted that PykF expression might be stimulated in the presence of allantoin, and this was indeed the case. Allantoin is a diureide derived from uric acid; itself a product of purine degradation. DNA-derived purines can be abundant in the airways of people with cystic fibrosis (CF), which is a common infection niche colonized by *P. aeruginosa* (Kumar et al., 2019) and indeed, these compounds can become abundant enough to support the appearance of auxotrophs defective in purine biosynthesis (Al Mahmud et al., 2021).

But why encode a dedicated second pyruvate kinase isozyme ($PykF_{PA}$) when the organism already contains a similarly bioactive isozyme ($PykA_{PA}$) which appears to be expressed under most conditions? The answer to this question is not yet clear, although we note that during growth on allantoin as a sole

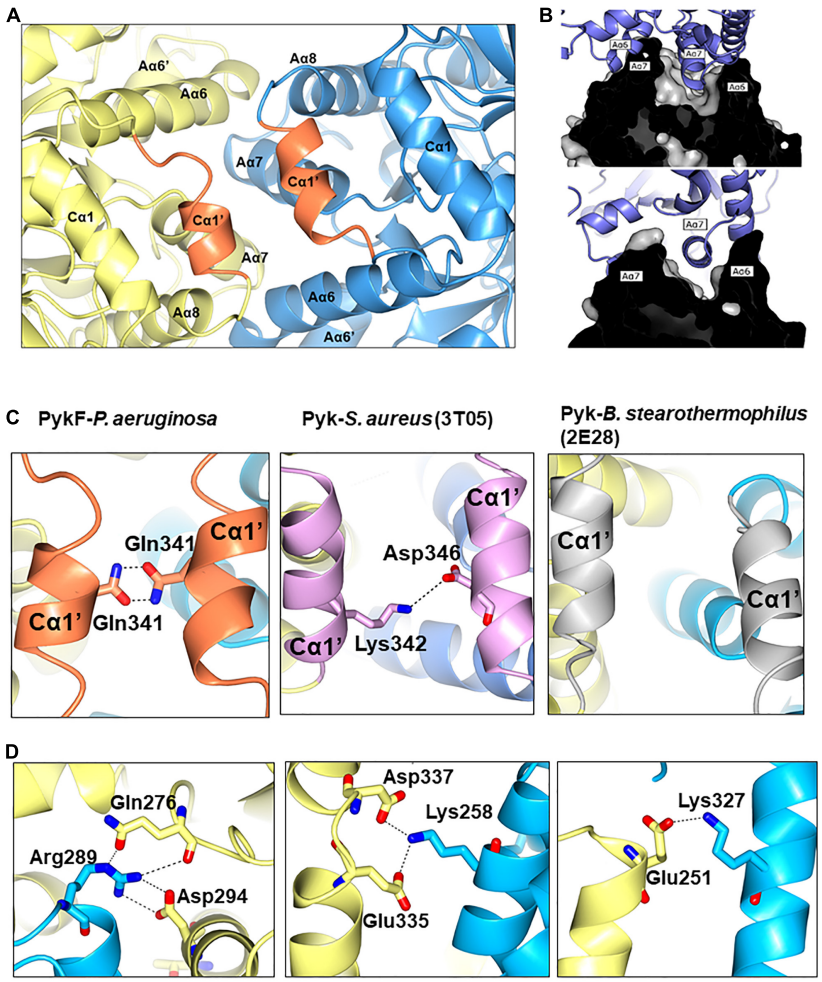

FIGURE 6 | The A-A interface of PykF. **(A)** Secondary structures present at the A-A interface in PykF. The Cα1′ helices are shown in coral. **(B)** The interlocking of α-helices Aα6 and Aα7 at the A-A interface (upper and lower panels show a cross-section through the interface at different tilt angles). **(C)** Close-up view of the interactions at the Cα1′-Cα1′ interspace in bacterial species that have a Cα1′-like structure. **(D)** Close-up view of the A-A interface in PykF showing salt bridge formation across the interface. Of note, the A-A interface of *E. coli* PykF does not contain a Cα1′-like structure or salt bridges.

carbon source, the *pykF* mutant displayed a growth defect relative to the *pykA* mutant (**Supplementary Figure 1**), which strongly suggests that the two isozymes are not equivalent. One possibility is that one or more of the intermediates that are generated during growth on allantoin may differentially inhibit $PykA_{PA}$ but not $PykF_{PA}$. One obvious candidate in this regard would be hydroxypyruvate (derived from the spontaneous non-enzymatic isomerization of tartronate semialdehyde–the predicted product of the glyoxylate carboligase-catalyzed reaction). However, hydroxypyruvate had no significant differential effect on the activity of $PykA_{PA}$ and $PykF_{PA}$ (*data now shown*), so we infer that some other intermediate is likely responsible. If the function of $PykF_{PA}$ is indeed to compensate for the inhibition of $PykA_{PA}$ during growth on allantoin, this would also explain why the two enzymes have very similar regulatory properties.

The *pykF* ORF encodes a functional pyruvate kinase with kinetic parameters roughly comparable with those of $PykA_{PA}$. Purified $PykF_{PA}$ and $PykA_{PA}$ were also activated by a broadly similar set of allosteric regulators. Notably, and although the PykF sub-family of PK isozymes were originally functionally designated as being regulated by fructose 1,6-*bis*phosphate, this metabolite had little impact on the activity of $PykF_{PA}$. Similarly, whereas the PykA family of isozymes were originally designated thus because they are regulated by AMP, this molecule had no impact on the activity of $PykA_{PA}$ (Abdelhamid et al., 2019) although it is a moderate activator of $PykF_{PA}$. These data may suggest that assignation of a PK isozyme into the "PykA" or "PykF" sub-family, which nowadays, is largely based on sequence analyses, is a convenience that does not necessarily have any associated functional significance. However, the insensitivity of $PykF_{PA}$ (and also $PykA_{PA}$) to fructose 1,6-*bis*phosphate may also have a structural explanation. Analysis of the fructose 1,6-*bis*phosphate-activated yeast PK revealed that the negatively charged phosphate moiety at the 1 position of the sugar ring in the regulator molecule interacts with a positively charged residue (arginine) located on the nearby Cα4 (Jurica et al., 1998). Other

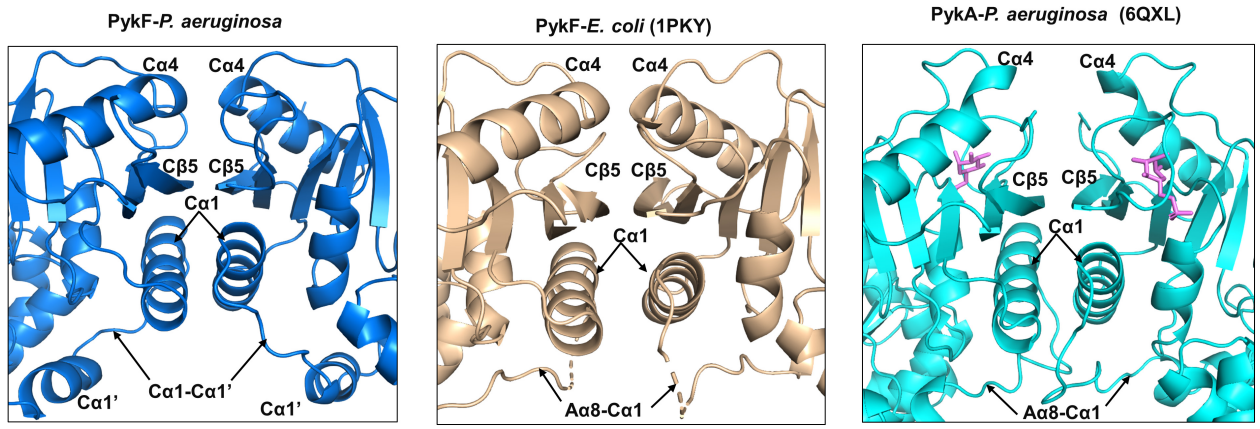

FIGURE 7 | Secondary structures of the C-C interface of $PykF_{PA}$ (blue), $PykF_{EC}$ (wheat) and $PykA_{PA}$ (cyan). The diagram shows that the C-C interface in $PykF_{PA}$ adopts almost the same configuration as the C-C interface in $PykF_{EC}$, likely due to the absence of bound regulator in the allosteric site. The G6P bound to $PykA_{PA}$ is shown as pink sticks.

fructose 1,6-*bis*phosphate-activated PykF isoforms also contain candidate positively charged residue(s) on Cα4 at the equivalent position (**Supplementary Figure 8**). By contrast, the Cα4 (residues 425–438) of $PykF_{PA}$ lacks a positively charged residue at this position on Cα4, likely accounting for its insensitivity to fructose 1,6-*bis*phosphate. This insensitivity to fructose 1,6-*bis*phosphate makes good physiological sense, since, due to the absence of phosphofructokinase (and thus, a conventional EMP pathway) in PA, the only time this intermediate will accumulate is during gluconeogenesis. Clearly, it would be wasteful to stimulate EDP glycolysis in these circumstances.

One of the main differences between the structure of $PykF_{PA}$ and the pyruvate kinases from other Proteobacteria is that $PykF_{PA}$ contains a Cα1′ helix. In many species, Cα1′ is replaced by a long uninterrupted loop (the Aα8-Cα1 loop) connecting the A- and C-domains (**Supplementary Figure 9**). Some Firmicutes also have a Cα1′-like structure (**Figure 6C**), although with a diverse amino acid sequence (**Supplementary Figure 4**). This indicates that the function of Cα1′ is likely species-specific. In $PykA_{PA}$, the Aα8-Cα1 loop has been implicated in transmission of the conformational signal from the allosteric site to the active site (Abdelhamid et al., 2019), so Cα1′ is located at a strategically important site in the enzyme (**Figures 6**, **7**). However, abolition of the presumed reciprocal H-bonds between the side chain of residue Gln341 on each protomer (H-bonds which apparently stabilize Cα1′-Cα1′ interactions between protomers) had little impact on the activity or G6P-dependent regulation of the enzyme, so the functional role(s), if any, of this secondary structure remain unclear.

Analysis of the C-C interface in apo-$PykF_{PA}$ shows that the ring loop between Cβ4 and Cβ5 is not a part of the interface. This contrasts with the same structure in apo-$PykF_{EC}$ and in the pyruvate kinase from *M. tuberculosis* (Pyk_{Mtb}). This is apparently due to the partial retraction of the ring loop from the interface and its movement toward the allosteric site, a feature that is presumably attributable to the presence of Pro459 (**Figure 5C**). A possible role for the other ring loop-flanking proline, Pro455, in this is made less likely by the fact that whereas $PykF_{Ec}$ lacks a proline at the equivalent position, Pyk_{Mtb} retains one. Nevertheless, the conformational importance of Pro455 is confirmed by the fact that the mutant Pro455Ala $PykF_{PA}$ protein is locked into an essentially constitutively active configuration. By contrast, mutation of Pro459 to Ala apparently locked the enzyme into a non-activatable (by G6P) state. We speculate that in this mutant protein, the ring loop engages in other interactions that prevent it from fully folding over the G6P-binding site following interaction with the ligand, thereby blocking the downstream conformational transitions leading to activation.

The A-A inter-protomer space of $PykF_{PA}$ is distinguished from that in $PykF_{EC}$ and Pyk_{Mtb} by the presence of the Cα1′ helices, and by bonding of the Aα8-Cα1′ loop with Aα6 (**Figure 8**). In light of this, it is tempting to extrapolate a general mechanism that may explain the allosteric regulation of $PykF_{PA}$. Upon binding of a regulator molecule in the allosteric pocket of $PykF_{PA}$, the ring loop folds down across the bound ligand, along similar lines to what is observed in G6P-bound $PykA_{PA}$ (Zhong et al., 2017; Abdelhamid et al., 2019). This movement of the ring loop would be expected to induce rearrangement of the structures at the C-C interface, including breaking of Cα4-Cα4 interactions and building of a Cα1-Cα1 interaction. These proposed changes at the C-C interface are common in the allosteric regulation of many bacterial and non-bacterial pyruvate kinases (Mattevi et al., 1996; Jurica et al., 1998; Abdelhamid et al., 2019) and naturally lead to a set of inferred downstream changes in which the shifting of Cα1 toward the C-C interface "pulls" on the Cα1-Cα1′ loop, Cα1′ helix, Aα8-Cα1′ loop and/or Aα8 helix. These movements of the Aα8-Cα1′ loop and/or Aα8 away from the A-A interface would free Aα6 and the Aα6′ active site helix to move (accounting for the change in relative orientation of the A- and B-domains on the protein, leading to closure of the active site) and to promote new interactions at the A-A interface. Such a set of proposed conformational changes would provide a direct structural pathway linking events at the ligand (effector) binding site and the active site. Consistent with this model, recruitment

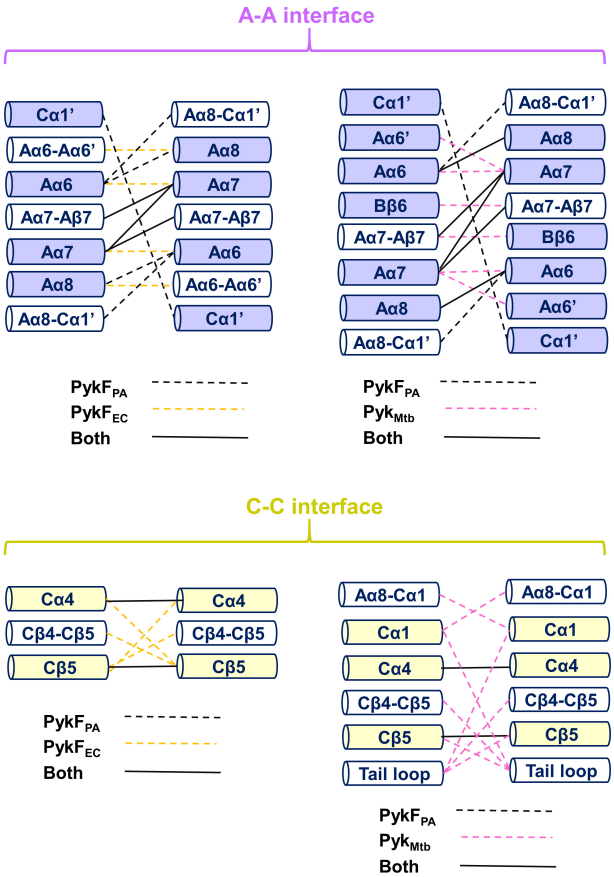

FIGURE 8 | The inter-protomer interfaces in PykF. The top diagram shows a comparison between the A-A interface in PykF$_{PA}$, and (left) PykF$_{EC}$ and (right) Pyk$_{Mtb}$. The bottom panel shows a comparison between the C-C interface in PykF$_{PA}$ and (left) PykF$_{EC}$ and (right) Pyk$_{Mtb}$. Interactions unique to PykF$_{PA}$ (black dashed lines), PykF$_{EC}$ (yellow dashed lines), and Pyk$_{Mtb}$ (pink dashed lines) are shown. Interactions present in PykF$_{PA}$ and any of the two structures are shown as solid black lines.

of a Cα1′-like helix to the C-C interface has been observed before upon occupation of the allosteric site in a yeast pyruvate kinase by a regulator (Jurica et al., 1998). However, these proposed changes do not account for the extreme apparent "locked on" and "locked off" phenotypes of the ring loop Pro→Ala mutants. They also fail to take into account the fact that the most potent regulators of PykF$_{PA}$ are PPP sugars with linear (not ring-like) configurations, which may or may not bind to the inferred G6P-binding site on the protein; an issue that we are currently investigating.

In summary, we present here the structure, function and regulation of a second pyruvate kinase isoform, PykF$_{PA}$, from *P. aeruginosa*. Unlike the PykF$_{Ec}$ and PykA$_{Ec}$ isoforms in *E. coli*, which carry out essentially the same "metabolic job" but under different conditions of oxygen availability (Zhao et al., 2017), in *P. aeruginosa*, it is clear that PykA$_{PA}$ is "the main" pyruvate kinase employed under most growth conditions, and that PykF$_{PA}$ has a more dedicated role in allantoin degradation. Crucially, our structural and mechanistic data indicate that the specific nature of the "ring loop" interactions around the presumed G6P-binding site in PykF$_{PA}$ introduce a hitherto unexpected layer of complexity into our understanding of how allosteric transitions are accomplished. Indeed, our future efforts are aimed at trying to obtain the crystal structure of the "locked on" and "locked off" conformers, and in examining how the more potent (than G6P) PykF$_{PA}$ and PykA$_{PA}$ allosteric regulators work.

MATERIALS AND METHODS

PykF Expression

PW8308 (a Tn:*pykA* mutant) and PW3705 (a Tn:*pykF* mutant) were obtained from the UWGC *P. aeruginosa* mutant bank. The Tn insertion in each mutant has been previously confirmed (Abdelhamid et al., 2019). A single colony of each relevant strain (wild-type PAO1, the *pykA* mutant, and the *pykF* mutant) was picked and used to inoculate 10 mL LB. The cultures were grown overnight at 37°C on a rotating drum. The cells were then pelleted (3200 × *g*, 20°C, 5 min) and washed three times in 10 mL sterile PBS. The cells were then inoculated 200 mL M9 minimal media containing either glucose (14 mM) or allantoin (21 mM) or a combination of both carbon sources, to an initial OD_{600} of 0.05. These concentrations of each carbon source were chosen because they contain the same molar number of carbon atoms. The cultures were incubated for 24 h in orbital shaker at 37°C with good aeration (200 rpm). The cells were then pelleted by sedimentation (3200 × *g*, 4°C, 10 min) and resuspended in 2 mL lysis buffer [comprising 50 mM Tris–HCl (pH 7.5), 400 mM NaCl, 10 mM imidazole, 5% (v/v) glycerol and one EDTA-free protease inhibitor cocktail per 50 mL buffer]. The samples were sonicated on ice to completion and clarified by centrifugation (14,600 × *g*, 4°C, 5 min). The protein concentration in the clarified extract was quantified using the Bradford Assay (BSA standard). Samples (20 μg protein per lane) were then denatured in SDS sample buffer and resolved by SDS-PAGE (9% polyacrylamide gels). Following PAGE, the proteins were transferred to immobilon-FL PVDF membranes (Merck Millipore) using a Bio-Rad *Trans*-Blot Turbo (mixed MW program; 2.5 A, 7 min for 2 mini gels). The membranes were washed 3× for 5 min in phosphate-buffered saline containing 0.1% (v/v) TWEEN-20 and blocked overnight in the same buffer containing 5% w/v skimmed milk. The primary antibody [anti-PykA (1:2000) or anti-PykF (1:3000) (Abdelhamid et al., 2019)] was incubated with each membrane for 60 min at room temperature. The membranes were then washed 3× for 5 min in PBS-TWEEN wash buffer before addition of the secondary antibody [IRDye 800CW Goat anti-Rabbit (LI-COR), 1:15,000]. After 60 min, the membranes were washed 3× in PBS-TWEEN and imaged using a ChemiDoc MP Imaging System (Bio-Rad).

Cloning, Overexpression and Purification of PykF

PykF was over-expressed in *E. coli* strain BL21 (DE3) containing plasmid pET-19m (*pykF*) and purified as previously described (Abdelhamid et al., 2019).

Kinetic Analysis of Purified PykF

Pyruvate kinase activity was measured using a lactate dehydrogenase (LDH)-coupled assay following our previous protocol for purified PykA (Abdelhamid et al., 2019) except that unless otherwise stated, purified PykF was added to a final concentration of 0.25 μg/mL to start the reactions. Regulator screens were also carried out as previously described (Abdelhamid et al., 2019). In all experiments, regulators were added at 1 mM final concentration except for R5P, X5P, and RL5P which were used at 0.15, 0.5, and 0.5 mM, respectively. GraphPad prism 7 was used to analyze the data and to extract the kinetic constants. All experiments were carried out in triplicate. Raw and processed kinetic data are provided in **Supplementary Tables 3**, **4**.

Analytical Ultracentrifugation

Analytical ultracentrifugation analyses were carried out as previously described (Abdelhamid et al., 2019). Data analysis and calculations of buffer viscosity, protein partial specific volumes and frictional rations were done using SEDFIT (Schuck, 2000) and SEDNTERP (Hayes et al., 1995).

Crystallization of PykF

PykF was crystallized using the sitting drop vapor diffusion method. MRC 2-drop plates (Swissci) were used and solutions were dispensed using the Mosquito robotics system (SPT Labtech). Purified PykF [29 mg/mL in 20 mM Tris–HCl, 100 mM NaCl, 5% (v/v) glycerol, 1 mM DTT, 0.1 mM EDTA, 20 mM $MgCl_2$, 200 mM KCl, 2 mM PEP (pH 7.5)] was mixed 1:1 (200 nL each) with the reservoir buffer containing 25% (w/v) PEG6000 and 0.1 M Hepes (pH 7.5). Crystals grew within 1 week. The crystals were mounted on nylon loops and cryoprotected in mother liquor supplemented with 40% (v/v) glycerol before being flash frozen in liquid N_2.

X-ray Diffraction, Structure Determination and Refinement

Diffraction data were collected at the Diamond Light Source (Didcot, United Kingdom) on beamline IO4-1 (MX14043-47). The PykF structure was obtained by molecular replacement using Phaser MR (McCoy et al., 2007) and a PykF ensemble generated by the Swiss model (Waterhouse et al., 2018) as a structural template. Coot (Emsley et al., 2010) was used for model building, and refinement was carried out using Phenix.refine (Adams et al., 2010). The overall model of PykF was acceptable except that the electron density signal was weak at the Cβ3 strand (now modeled as a loop) and the three terminal residues (now unmodelled) of chain A. The structural coordinates of PykF were deposited in the PDB with the accession code 7OO1. PDBePISA (Krissinel and Henrick, 2007) was used for analysis of the tetramer and ligand interfaces. Figures were generated using CCP4mg (McNicholas et al., 2011).

Amino Acid Sequence Analysis

Amino acid sequences were extracted from UniProt in FASTA format, aligned by Clustal Omega (Goujon et al., 2010; Sievers et al., 2014) and formatted for display using ESPript (Robert and Gouet, 2014).

Site-Directed Mutagenesis

Site-directed mutagenesis (Q341A, P455A, and P459A mutants) was carried out by overlap extension PCR using pET-19m (*pykF*) as a template. The *pykF* cloning primers and an extra pair of overlap primers were designed and used for site-directed mutagenesis (**Supplementary Table 1**). Briefly, in the first PCR step, the 5′ region of the *pykF* gene was amplified using the *pykF* forward cloning primer and the corresponding reverse overlap primer, and the 3′ region was amplified using the *pykF* reverse cloning primer and relevant forward overlap primer. The purified 5′ and 3′ region PCR products were subsequently mixed and used as a template for PCR -amplification using the *pykF* cloning primers. The resulting PCR product was ligated to pET-19m using T4 DNA ligase (NEB). Each mutation was confirmed by DNA sequencing. The expression and purification of the mutated PykF proteins was the same as for the wild-type protein (Abdelhamid et al., 2019).

DATA AVAILABILITY STATEMENT

The datasets presented in this study can be found in online repositories. The names of the repository/repositories and accession number(s) can be found below: http://www.wwpdb.org/, PDB 7OO1.

AUTHOR CONTRIBUTIONS

YA carried the kinetic and regulatory analysis of the wild-type protein, obtained the crystallographic data, and drafted the manuscript. MWa carried out the site-directed mutagenesis and subsequent characterization of the mutant proteins. SP carried out the expression analyses. PB assisted in phasing and solving the crystal structure. MWe conceived of the study, analyzed the data, and assisted in preparation of the manuscript. XC and TR assisted with the structural analysis. All authors contributed to the article and approved the submitted version.

FUNDING

This work was initiated during and part-funded by a grant from the BBSRC (BB/M019411/1). YA was funded by a Ph.D. studentship from the Yousef Jameel Foundation. MWa is supported by the UK Cystic Fibrosis Trust as part of SRC017. XC was funded by a scholarship from IDB-Malaysia.

SUPPLEMENTARY MATERIAL

The Supplementary Material for this article can be found online at: https://www.frontiersin.org/articles/10.3389/fmicb.2021.790742/full#supplementary-material

REFERENCES

Abdelhamid, Y., Brear, P., Greenhalgh, J., Chee, X., Rahman, T., and Welch, M. (2019). Evolutionary plasticity in the allosteric regulator binding site of pyruvate kinase isoform PykA from *Pseudomonas aeruginosa*. *J. Biol. Chem.* 294, 15505–15516. doi: 10.1074/jbc.RA119.009156

Adams, P. D., Afonine, P. V., Bunkóczi, G., Chen, V. B., Davis, I. W., Echols, N., et al. (2010). PHENIX: a comprehensive Python-based system for macromolecular structure solution. *Acta Crystallogr. Sect. D Biol. Crystallogr.* 66, 213–221. doi: 10.1107/S0907444909052925

Al Mahmud, H., Baishya, J., and Wakeman, C. A. (2021). interspecies metabolic complementation in cystic fibrosis pathogens via purine exchange. *Pathogens* 10:146. doi: 10.3390/pathogens10020146

Al-Zaid Siddiquee, K., Arauzo-Bravo, M. J., and Shimizu, K. (2004). Metabolic flux analysis of pykF gene knockout *Escherichia coli* based on 13C-labeling experiments together with measurements of enzyme activities and intracellular metabolite concentrations. *Appl. Microbiol. Biotechnol.* 63, 407–417. doi: 10.1007/s00253-003-1357-9

Baek, Y. H., and Nowak, T. (1982). Kinetic evidence for a dual cation role for muscle pyruvate kinase. *Arch. Biochem. Biophys.* 217, 491–497. doi: 10.1016/0003-9861(82)90529-X

Bücker, R., Heroven, A. K., Becker, J., Dersch, P., and Wittmann, C. (2014). The pyruvate-tricarboxylic acid cycle node: a focal point of virulence control in the enteric pathogen Yersinia pseudotuberculosis. *J. Biol. Chem.* 289, 30114–30132. doi: 10.1074/jbc.M114.581348

Bumann, D., and Schothorst, J. (2017). Intracellular *Salmonella* metabolism. *Cell. Microbiol.* 19:e12766. doi: 10.1111/cmi.12766

Cusa, E., Obradors, N., Baldomà, L., Badía, J., and Aguilar, J. (1999). Genetic analysis of a chromosomal region containing genes required for assimilation of allantoin nitrogen and linked glyoxylate metabolism in *Escherichia coli*. *J. Bacteriol.* 181, 7479–7484. doi: 10.1128/jb.181.24.7479-7484.1999

Drechsler, E. R., Boyer, P. D., and Kowalsky, A. G. (1959). The catalytic activity of carboxypeptidase-degraded aldolase. *J. Biol. Chem.* 234, 2627–2634.

Emsley, P., Lohkamp, B., Scott, W. G., and Cowtan, K. (2010). Features and development of Coot. *Acta Cryst.* 66, 486–501. doi: 10.1107/S0907444910007493

Garcia-Olalla, C., and Garrido-Pertierra, A. (1987). Purification and kinetic properties of pyruvate kinase isoenzymes of *Salmonella* typhimurium. *Biochem. J.* 241, 573–581. doi: 10.1042/BJ2410573

Goujon, M., McWilliam, H., Li, W., Valentin, F., Squizzato, S., Paern, J., et al. (2010). A new bioinformatics analysis tools framework at EMBL-EBI. *Nucleic Acids Res.* 38, W695–W699. doi: 10.1093/nar/gkq313

Hayes, D., Laue, T., and Philo, J. (1995). *Program Sednterp: Sedimentation Interpretation Program*. Thousand Oaks, CA: Alliance Protein Laboratories.

Hofmann, J., Heider, C., Li, W., Krausze, J., Roessle, M., and Wilharm, G. (2013). Recombinant production of Yersinia enterocolitica pyruvate kinase isoenzymes PykA and PykF. *Protein Expr. Purif.* 88, 243–247. doi: 10.1016/j.pep.2013.01.010

Jurica, M. S., Mesecar, A., Heath, P. J., Shi, W., Nowak, T., and Stoddard, B. L. (1998). The allosteric regulation of pyruvate kinase by fructose-1,6-bisphosphate. *Structure* 6, 195–210.

Kachmar, J., and Boyer, P. (1953). Kinetic analysis of enzyme reactions. II. The potassium activation and calcium inhibition of pyruvic phosphoferase. *J. Biol. Chem.* 200, 669–682.

Kayne, F. J. (1973). 11 Pyruvate Kinase. *Enzymes* 8, 353–382. doi: 10.1016/S1874-6047(08)60071-2

Kersters, K., and De Ley, J. (1968). The occurrence of the Entner-Doudoroff pathway in bacteria. *Antonie Leeuwenhoek* 34, 393–408. doi: 10.1007/BF02046462

Kohlstedt, M., and Wittmann, C. (2019). GC-MS-based 13 C metabolic fl ux analysis resolves the parallel and cyclic glucose metabolism of *Pseudomonas* putida KT2440 and *Pseudomonas aeruginosa* PAO1. *Metab. Eng.* 54, 35–53. doi: 10.1016/j.ymben.2019.01.008

Kovachevich, R., and Wood, W. A. (1955a). Carbohydrate metabolism by *Pseudomonas* fluorescens. III. Purification and properties of a 6-phosphogluconate dehydrase. *J. Biol. Chem.* 213, 745–756. doi: 10.1016/s0021-9258(18)98206-2

Kovachevich, R., and Wood, W. A. (1955b). Carbohydrate metabolism by *Pseudomonas* fluorescens. IV. Purification and properties of 2-keto-3-deoxy-6-phosphogluconate aldolase. *J. Biol. Chem.* 213, 757–767.

Krissinel, E., and Henrick, K. (2007). Inference of macromolecular assemblies from crystalline state. *J. Mol. Biol.* 372, 774–797. doi: 10.1016/j.jmb.2007.05.022

Kumar, S. S., Penesyan, A., Elbourne, L. D. H., Gillings, M. R., and Paulsen, I. T. (2019). Catabolism of nucleic acids by a cystic fibrosis *Pseudomonas aeruginosa* isolate: an adaptive pathway to cystic fibrosis sputum environment. *Front. Microbiol.* 10:1199. doi: 10.3389/fmicb.2019.01199

Laughlin, L. T., and Reed, G. H. (1997). The monovalent cation requirement of rabbit muscle pyruvate kinase is eliminated by substitution of lysine for glutamate 117. *Arch. Biochem. Biophys.* 348, 262–267. doi: 10.1006/abbi.1997.0448

Lessie, T. G., and Phibbs, P. V. (1984). Alternative pathways of carbohydrate utilization in pseudomonads. *Annu. Rev. Microbiol.* 38, 359–388. doi: 10.1146/annurev.mi.38.100184.002043

Martínez-Solano, L., Macia, M. D., Fajardo, A., Oliver, A., and Martinez, J. L. (2008). Chronic *Pseudomonas aeruginosa* infection in chronic obstructive pulmonary disease. *Clin. Infect. Dis.* 47, 1526–1533. doi: 10.1086/593186

Mattevi, A., Bolognesi, M., and Valentini, G. (1996). The allosteric regulation of pyruvate kinase. *FEBS Lett.* 389, 15–19.

McCoy, A. J., Grosse-Kunstleve, R. W., Adams, P. D., Winn, M. D., Storoni, L. C., and Read, R. J. (2007). Phaser crystallographic software. *J. Appl. Crystallogr.* 40, 658–674. doi: 10.1107/S0021889807021206

McNicholas, S., Potterton, E., Wilson, K. S., and Noble, M. E. M. (2011). Presenting your structures: the CCP4mg molecular-graphics software. *Acta Crystallogr. Sect. D Biol. Crystallogr.* 67, 386–394. doi: 10.1107/S0907444911007281

Nikel, P. I., Chavarría, M., Fuhrer, T., Sauer, U., and de Lorenzo, V. (2015). *Pseudomonas putida* KT2440 strain metabolizes glucose through a cycle formed by enzymes of the entner-doudoroff, embden-meyerhof-parnas, and pentose phosphate pathways. *J. Biol. Chem.* 290, 25920–25932. doi: 10.1074/jbc.M115.687749

Noy, T., Vergnolle, O., Hartman, T. E., Rhee, K. Y., Jacobs, W. R., Berney, M., et al. (2016). Central role of pyruvate kinase in carbon co-catabolism of mycobacterium tuberculosis. *J. Biol. Chem.* 291, 7060–7069. doi: 10.1074/jbc.M115.707430

Oria-Hernández, J., Riveros-Rosas, H., and Ramírez-Sílva, L. (2006). Dichotomic phylogenetic tree of the pyruvate kinase family. *J. Biol. Chem.* 281, 30717–30724. doi: 10.1074/jbc.M605310200

Peekhaus, N., and Conway, T. (1998). What's for dinner?: entner-doudoroff metabolism in *Escherichia coli*. *J. Bacteriol.* 180, 3495–3502. doi: 10.1128/JB.180.14.3495-3502.1998

Ponce, E., Flores, N., Martinez, A., Valle, F., and Bolívar, F. (1995). Cloning of the two pyruvate kinase isoenzyme structural genes from *Escherichia coli*: the relative roles of these enzymes in pyruvate biosynthesis. *J. Bacteriol.* 177, 5719–5722. doi: 10.1128/JB.177.19.5719-5722.1995

Preston, M. J., Seed, P. C., Toder, D. S., Iglewski, B. H., Ohman, D. E., Gustin, J. K., et al. (1997). Contribution of proteases and LasR to the virulence of *Pseudomonas aeruginosa* during corneal infections. *Infect. Immun.* 65, 3086–3090. doi: 10.1128/iai.65.8.3086-3090.1997

Robert, X., and Gouet, P. (2014). Deciphering key features in protein structures with the new ENDscript server. *Nucleic Acids Res.* 42, W320–W324. doi: 10.1093/nar/gku316

Romano, A. H., and Conway, T. (1996). "Evolution of carbohydrate metabolic pathways," in *Research in Microbiology*, eds T. Msadek, C. Beloin, and D. Cabanes (Issy-les-Moulineaux: Elsevier Masson SAS), 448–455. doi: 10.1016/0923-2508(96)83998-2

Rose, I. A. (1970). Stereochemistry of pyruvate kinase, pyruvate carboxylase, and malate enzyme reactions. *J. Biol. Chem.* 245, 6052–6056.

Schuck, P. (2000). Size-distribution analysis of macromolecules by sedimentation velocity ultracentrifugation and lamm equation modeling. *Biophys. J.* 78, 1606–1619. doi: 10.1016/S0006-3495(00)76713-0

Seeholzer, S. H., Jaworowski, A., and Rose, I. A. (1991). Enolpyruvate: chemical determination as a pyruvate kinase intermediate. *Biochemistry* 30, 727–732. doi: 10.1021/bi00217a022

Sievers, F., Wilm, A., Dineen, D., Gibson, T. J., Karplus, K., Li, W., et al. (2014). Fast, scalable generation of high-quality protein multiple sequence alignments using Clustal Omega. *Mol. Syst. Biol.* 7, 539–539. doi: 10.1038/msb.2011.75

Temple, L. M., Sage, A. E., Schweizer, H. P., and Phibbs, P. V. (1998). "Carbohydrate catabolism in *Pseudomonas aeruginosa*," in *Pseudomonas*, ed. T. C. Montie (Boston, MA: Springer), 35–72. doi: 10.1007/978-1-4899-0120-0_2

Turner, K. H., Everett, J., Trivedi, U., Rumbaugh, K. P., and Whiteley, M. (2014). Requirements for *Pseudomonas aeruginosa* acute burn and chronic surgical wound infection. *PLoS Genet.* 10:e1004518. doi: 10.1371/journal.pgen.1004518

Valentini, G., Iadarola, P., Somani, B. L., and Malcovati, M. (1979). Two forms of pyruvate kinase in *Escherichia coli* a comparison of chemical and molecular properties. *Biochim. Biophys. Acta Enzymol.* 570, 248–258. doi: 10.1016/0005-2744(79)90145-1

Waterhouse, A., Bertoni, M., Bienert, S., Studer, G., Tauriello, G., Gumienny, R., et al. (2018). SWISS-MODEL: homology modelling of protein structures and complexes. *Nucleic Acids Res.* 46, W296–W303. doi: 10.1093/nar/gky427

Waygood, E. B., and Sanwal, B. D. (1974). The control of pyruvate kinases of *Escherichia coli*. I. Physicochemical and regulatory properties of the enzyme activated by fructose 1,6-diphosphate. *J. Biol. Chem.* 249, 265–274.

Waygood, E. B., Mort, J. S., and Sanwal, B. D. (1976). The control of pyruvate kinase of *Escherichia coli*. Binding of substrate and allosteric effectors to the enzyme activated by fructose 1,6-bisphosphate. *Biochemistry* 15, 277–282. doi: 10.1021/bi00647a006

Waygood, E. B., Rayman, M. K., and Sanwal, B. D. (1975). The control of pyruvate kinases of *Escherichia coli*. II. Effectors and regulatory properties of the enzyme activated by ribose 5-phosphate. *Can. J. Biochem.* 53, 444–454. doi: 10.1139/o75-061

Wooll, J. O., Friesen, R. H., White, M. A., Watowich, S. J., Fox, R. O., Lee, J. C., et al. (2001). Structural and functional linkages between subunit interfaces in mammalian pyruvate kinase. *J. Mol. Biol.* 312, 525–540. doi: 10.1006/jmbi.2001.4978

Zhao, C., Lin, Z., Dong, H., Zhang, Y., and Li, Y. (2017). Reexamination of the physiological role of PykA in *Escherichia coli* revealed that it negatively regulates the intracellular ATP levels under anaerobic conditions. *Appl. Environ. Microbiol.* 83, e316–e317. doi: 10.1128/AEM.00316-17

Zhong, W., Cui, L., Goh, B. C., Cai, Q., Ho, P., Chionh, Y. H., et al. (2017). Allosteric pyruvate kinase-based "logic gate" synergistically senses energy and sugar levels in Mycobacterium tuberculosis. *Nat. Commun.* 8:1986. doi: 10.1038/s41467-017-02086-y

Conflict of Interest: The authors declare that the research was conducted in the absence of any commercial or financial relationships that could be construed as a potential conflict of interest.

Publisher's Note: All claims expressed in this article are solely those of the authors and do not necessarily represent those of their affiliated organizations, or those of the publisher, the editors and the reviewers. Any product that may be evaluated in this article, or claim that may be made by its manufacturer, is not guaranteed or endorsed by the publisher.